

Structural relaxation of nanocrystalline PdAu alloy: Probing the spectrum of potential barriers

Cite as: J. Appl. Phys. **126**, 205102 (2019); <https://doi.org/10.1063/1.5121520>

Submitted: 25 July 2019 • Accepted: 02 November 2019 • Published Online: 22 November 2019

 Michael Johannes Deckarm,  Christian Braun and Rainer Birringer



View Online



Export Citation



CrossMark

ARTICLES YOU MAY BE INTERESTED IN

[Structural relaxation of nanocrystalline PdAu alloy: Mapping pathways through the potential energy landscape](#)

Journal of Applied Physics **127**, 125115 (2020); <https://doi.org/10.1063/1.5141525>

[Piezoelectric creep in LiNbO₃, PMN-PT and PZT-5A at low temperatures](#)

Journal of Applied Physics **126**, 204101 (2019); <https://doi.org/10.1063/1.5119351>

[Melting curve of vanadium up to 470 GPa simulated by ab initio molecular dynamics](#)

Journal of Applied Physics **126**, 205901 (2019); <https://doi.org/10.1063/1.5124520>



APL Quantum

CALL FOR APPLICANTS

Seeking Editor-in-Chief

Structural relaxation of nanocrystalline PdAu alloy: Probing the spectrum of potential barriers

Cite as: J. Appl. Phys. 126, 205102 (2019); doi: 10.1063/1.5121520

Submitted: 25 July 2019 · Accepted: 2 November 2019 ·

Published Online: 22 November 2019



Michael Johannes Deckarm,^{a)}  Christian Braun,^{b)}  and Rainer Birringer^{c)}

AFFILIATIONS

Department of Experimental Physics, Saarland University, Campus D2.2, 66123 Saarbrücken, Germany

^{a)}Electronic mail: michael.deckarm@nano.uni-saarland.de

^{b)}Electronic mail: c.braun@nano.uni-saarland.de

^{c)}Electronic mail: r.birringer@nano.uni-saarland.de

ABSTRACT

A commonality between nanocrystalline metals and metallic glasses is their dependence of structure and properties upon preparation history and postprocessing. Depending on preparation conditions, stored excess enthalpy and volume—relative to the crystalline ground state—can vary significantly. Annealing of material states of elevated enthalpy or volume induces structural relaxation and concomitant depletion of excess energy and volume. We analyzed the kinetics of volume relaxation in nanocrystalline PdAu alloys by partitioning the overall process into a set of independent and parallel reactions for arbitrary time-temperature protocols. The obtained spectra of kinetic parameters imply a complex relaxation behavior that violates time-temperature superposition and time aging-time superposition. The analysis will enable to reconstruct the effective energy landscape underlying the relaxation dynamics.

© 2019 Author(s). All article content, except where otherwise noted, is licensed under a Creative Commons Attribution (CC BY) license (<http://creativecommons.org/licenses/by/4.0/>). <https://doi.org/10.1063/1.5121520>

I. INTRODUCTION

It is well established that glassy materials (polymers, silica glasses, metallic glasses, and molecular systems) change their properties years after the time of manufacture. This slow change of material properties with time far from equilibrium was termed (physical) aging.^{1,2} The origin of the time scale for aging is related to the way of synthesizing and processing the materials. Glassy materials are usually generated by cooling the material fast enough to avoid crystallization so entering the regime of the supercooled liquid to eventually—when the temperature falls below the liquid-to-glass transition temperature T_g —condense into the state of an amorphous solid.^{3–5} This disordered matter resides in a non-equilibrium state that proceeds to spontaneously evolve toward a temporally distant equilibrium state (metastable, confined, or unconfined/true). During this course, the state variables of the system, e.g., volume or enthalpy, alter.² Concomitantly, it is observed that macroscopic properties, such as mechanical,^{6,7} transport,⁸ dielectric,⁹ etc., properties, change with time.¹ Aging affects these properties through changes in the respective relaxation times of microscopic processes manifesting the system's structural relaxation dynamics toward lower-energy states at a given

temperature.^{10,11} We note that there is a reverse process, termed rejuvenation,¹² entailing an evolution of materials into higher-energy states through application of external forces, e.g., thermomechanical processing or irradiation.^{13,14} An overwhelming wealth of literature related to these topics has been published by the glass community and has been surveyed and critically assessed over the years to leave a number of excellent review articles^{1,2,4,15–19} to the interested reader. Finally, we note that aging is a general phenomenon, which is not restricted to the glassy state but should be found in all kinds of disordered materials irrespective of their chemical nature and of their atomic structure or microstructure.²⁰

In this regard, nanocrystalline (NC) materials²¹ are candidate materials that should exhibit pronounced relaxation and associated aging phenomena. In contrast to amorphous materials, they are composed of ordered regions, the crystallites, which are separated by disordered interfaces. This microstructure is characterized by a structural correlation length, the grain size D .²² Creation of NC materials ordinarily results in nonequibrated material states,²³ where energy in excess to the crystalline ground state is mainly stored in the core regions of the interfaces which accommodate the atomic-site mismatch between abutting and differently oriented

crystal lattices.²⁴ Additional excess energy is related to crystal lattice distortions due to the mechanical interplay between interfaces and grain interior or defects in the interior of individual nanocrystals.^{25,26} In this work, we will focus on dilute solid solution PdAu NC metals and use the standard term grain boundaries (GBs) to denote the interfacial phase of NC metals. Since the interface area per unit volume of crystal scales as $1/D$, this is also true for the capacity to store excess energy in the network of GBs. Therefore, decreasing the grain size of NC metals to the low end of the nanoscale (≈ 10 nm) entails a stored excess energy comparable to glassy metals²⁷ and hence should reveal a rich variety of relaxation and aging phenomena.

Regarding the pertinent literature, GB relaxation in NC metals was studied in the nineties of the last century. This research was driven by conflicting results obtained for nominally the same material.²⁸ Using X-ray diffraction,²⁹ calorimetry,^{23,30} dilatometry,³¹ MD simulations,³² and HRTEM³³ to analyze GB relaxation, it turned out that energy and volume release went along with a reduction of atomic-site disorder in/at GBs whenever annealing temperatures were low enough to avoid grain growth. Hence, we may assume that the reported conflicting results are related to different synthesis protocols or different thermal history before measurement. A subsequent careful study on microstructural evolution during heat treatment of NC pure metals and alloys unveiled the interplay between GB relaxation, grain growth, GB segregation, and chemical ordering in a microstructural evolution map.³⁴ GB relaxation and its effect on plasticity, in particular, on strain rate sensitivity and on hardness was investigated in NC Fe.²⁸ Recently, the complex defect annealing kinetics in ultrafine-grained Cu and Ni were studied with special emphasis on extracting the GB excess volume³⁵ related to site mismatch in the core region of GBs and to their capability of acting as sinks and sources for zero- and one-dimensional lattice defects, e.g., vacancies, segregants, and dislocations, respectively. However, careful studies of long-term relaxation dynamics and related aging phenomena have been scarcely explored.^{30,36} Likewise, state-of-the-art analysis of relaxation data, based on simultaneous fitting of sets of relaxation data received from different time-temperature protocols, is missing.

It is the objective of this study to analyze the kinetics of relaxation processes in NC PdAu alloys that are initiated by applying different time-temperature protocols. In particular, we investigate volume (length) release, a macroscopic quantity that directly couples to structural changes related to microstructure and interatomic distances. The epistemic goal of this work will focus on extracting the spectrum of kinetic parameters that are at the root of the relaxation dynamics and constitute an essential part of the underlying potential energy surface. As a practical purpose, kinetic parameters may be useful to predict process rates and material reliability/performance.

The realm of enthalpy and volume relaxation is a longstanding issue in amorphous materials so that, not surprisingly, many concepts and terminology have been introduced and set by this field. Therefore, the following paragraphs are devoted to address nomenclature issues and deliver a framework, which enables to draw links between metallic glasses and NC metals at the low end of the nanoscale.

II. BASIC CONCEPTS

To define the scope of the problem, we refer to the canonical glass-science diagram⁴ shown in Fig. 1. It illustrates how extensive quantities such as enthalpy, volume, and entropy evolve when a liquid is cooled fast enough to supercool (regime A) then enter regime B where the liquid-to-glass transition takes place to eventually form an amorphous solid or glass in regime C upon further cooling. In regime A, the glass former is in internal equilibrium; therefore, no dependencies on preparation history are observed and whenever the crystal formation is prohibited the system behaves ergodic.

In regime C, the glass is restricted to a configurationally frozen state below T_{cf} —like a mechanically rigid solid—and exhibits essentially reversible behavior with respect to temperature changes. A remaining source of dynamics relates to fluctuations of atoms or molecules which are confined to rather loosely packed regions (nanoscale spatial heterogeneities) in metallic glasses. However, this so-called β - or Johari-Goldstein relaxations freeze by cooling far enough below T_g .³⁷

A variety of phenomena can be observed in regime B not least since the properties of the system depend on the preparation route

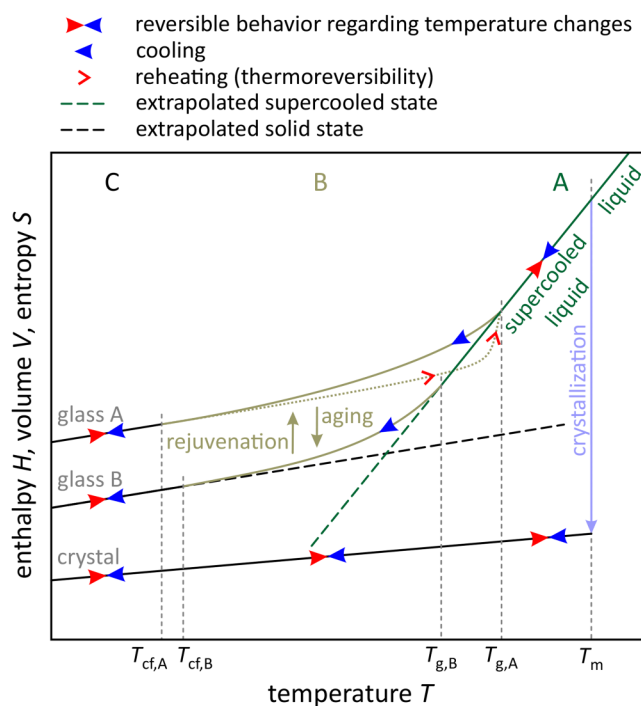


FIG. 1. Schematic of evolution of state variables enthalpy H , volume V , and entropy S of a glass upon cooling from above the melting temperature T_m . Below T_m , the thermodynamic stable state is the crystal. If crystallization is avoided, by applying suitable time-temperature protocols, a variety of glassy states (glass A, glass B, etc.) can be prepared. Regime A displays ergodic material behavior, and regime C represents the kinetically frozen glassy state. For details to transition regime B, we refer to the text.

into this regime, on the duration of the actual measurements at a given temperature, and on the time-temperature history before measurement. This relates to the fact that the system manifests degrees of freedom of atomic and molecular movement which promote its evolution toward equilibrium that is driven by a decrease of the free energy of the system. Many terms were coined to describe this behavior: relaxation, aging or aging dynamics, structural relaxation, enthalpy relaxation, enthalpy recovery, and physical aging to stress absence of chemical reactions like degradation, phase separation, clustering, or surface reactions with the environment.² Likewise, there are different terminologies for time (e.g., annealing, aging, and retardation time) and temperature (fictive and effective temperature)—this list does not qualify for completeness. Unfortunately, the use of nomenclature is rather nonuniform.

To clarify the terminology relevant to this study, we will introduce an adapted scheme to provide a framework for NC metals in Fig. 2. As for glasses, it depicts the crystalline ground state that entails genuine reversible behavior in all regimes below the melting temperature T_m , thus providing a common baseline for both types of material. Strictly speaking, the single crystalline material manifests the true equilibrium ground state. However, since we are not aware of any evidence suggesting that a single crystal can emerge from a coarse grained polycrystal, even by annealing just below the

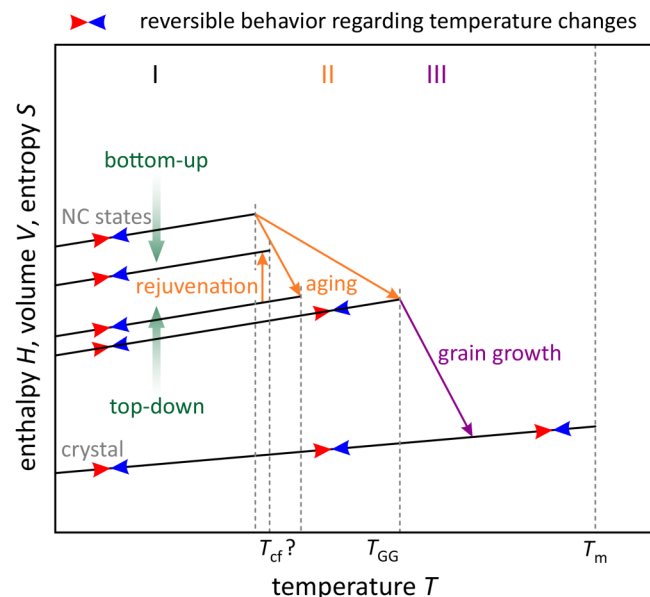


FIG. 2. Schematic of evolution of state variables enthalpy H , volume V , and entropy S of a nanocrystalline material as a function of temperature. The nanocrystalline states manifest elevated energies compared to the crystalline reference state. The green arrows indicate distinguished synthesis routes enabling to enter the nanocrystalline domain, either by energizing (top-down) or by deenergizing (bottom-up) bulk or atomic/molecular material states; the arrowheads symbolize direction, however, they are not meant to mark specific enthalpy values of nanocrystalline states. For details to the different regimes (I, II, and III), we refer to the text.

melting point, the coarse grained polycrystal is taken as a reference state for practical reasons.

Similar to glasses in regime C (Fig. 1), there exist multiple configurationally frozen and far out of equilibrium states at different levels of enthalpy (volume, entropy) in regime I (Fig. 2) in which the material behaves essentially reversible. Departure from equilibrium at the low end of the nanoscale is not only caused by the escalation of interfacial area and the inherent excess energy. There is a second energy contribution related to the fact that, depending on preparation and processing, the GBs themselves reside in nonequilibrium configurations. As an upper bound estimate, the specific excess energy stored in nonequilibrium GBs could be twice as large as the value of their locally equilibrated counterparts.²³

Increasing the temperature above T_{cf} leads to a reduction of free energy, which involves enthalpy release through structural relaxation (regime II) and with further increase of temperature grain growth (regime III). In NC metals, a strict separation of these processes generally fails.²⁵ Nevertheless, we can identify time-temperature settings which allow one to investigate the structural relaxation dynamics underlying enthalpy or volume release at practically constant grain size; a detailed analysis of this issue will be addressed in a follow-up paper.

In NC metals, the crystal lattices of nanocrystals and their conjoined GBs are in mechanical equilibrium requiring continuous stress σ across the interfaces. Because of the reduction of the effective elastic moduli of GBs relative to the grain interior,^{38,39} they are subjected to higher effective strains ε and thereby capable of storing higher energy densities $w = \sigma \cdot \varepsilon$ than the grain interiors. Moreover, molecular dynamics simulations reveal the presence of an inhomogeneous strain concentration in the immediate vicinity of interface regions of nanocrystals,^{40,41} which entails an even more pronounced concentration of stored energy at/near GBs. As a consequence, we expect the volume/enthalpy release in regime II to be dominated by interfacial relaxation dynamics which mainly involves structural rearrangement in the core region of GBs and a concomitant change of their defect character; a coupling of interfacial relaxation modes to the abutting nanocrystals can be regarded as a second order effect.

The transition from nanocrystallinity into the coarse grained state occurs beyond the temperature T_{GG} , which marks the onset of significant grain growth (regime III). Different modes of growth and kinetics deviating from classical curvature driven growth have been reported for NC metals.^{25,42–44} Summarizing the details of underlying mechanisms, addressing the possible coexistence of relaxation and growth, etc., is beyond the scope of this work.

The comparison between glasses and metals reveals a fundamental difference related to thermoreversibility: many glasses can be reheated without crystal formation or clustering to above T_g where they assume the state of an equilibrated supercooled liquid again.¹⁹ Thermoreversibility is completely absent in NC materials, since the abundance of nanocrystallites enforces the evolution of the system for any time-temperature protocol, that provides sufficient kinetics for GB boundary migration, toward the coarse grained equilibrium state.

Generating NC bulk materials⁴⁵ can be achieved by two different synthesis strategies: top-down or bottom-up. The

top-down approach (cf. Fig. 2) starts from coarse grained polycrystalline materials which are energized below T_{cf} , typically through cycled severe plastic deformation,⁴⁶ to evolve in a self-organized manner into a NC microstructure. Energy is stored as interfacial excess energy but also as strain energy associated with crystal lattice distortions and presence of high densities of dislocations and excess vacancies in the interior of the nanocrystallites. As expected, the concomitant stored excess enthalpy (volume, entropy, etc.) depends on the specific conditions of the preparation history.

In the bottom-up approach (cf. Fig. 2), nanoscale microstructures are grown by adding individual atoms to a substrate thereby forming a growing layer which preserves the nanoscale microstructure upon further accumulation of atoms or molecules. Alternatively, individual nanocrystallites are created followed by a transformation of their free surfaces to internal interfaces. In both scenarios, the high energy of the initial state (single atoms, nanometer-sized crystals) is reduced by generating solids with a high density of interfaces. Again, the amount of stored enthalpy depends on the specific preparation and processing conditions, which may vary significantly.

In what follows, we concentrate on the bottom-up approach and in particular on NC materials prepared by inert gas condensation (IGC). This process generates rather perfect nanocrystals in a He atmosphere which are collected and subsequently compacted in vacuum.²¹ IGC-prepared NC metals are distinguished by a random texture and a random interface orientation distribution function,⁴⁷ basically equiaxed grain shape and a lognormal grain size distribution function.²² Hence, they can be considered as prototypical random polycrystals, however, with enhanced localized stress and strain fluctuations due to the initial incompatibility of abutting crystallite shapes. Therefore, they seem predestined candidate materials to study nonequilibrium relaxation and related physical aging phenomena; the presence of pronounced anisotropies (texture) and/or macroscopic inhomogeneities would tremendously complicate the task.

Regarding nomenclature, we use the term annealing in its most general sense that is any time-temperature processing of specimens at elevated temperatures. This includes the commonly used isothermal and constant heating/cooling rate methods, as well as combinations thereof and nonlinear heating/cooling. During annealing, we measure the time evolution of volume (length) release, which is driven by free energy reduction of the system. This scenario has been labeled by alternative terms such as enthalpy recovery, physical aging, or (structural) relaxation. In this article, we will use the term structural relaxation to describe processes that reduce the free energy of the material system as well as the associated changes of physical properties.

III. METHODS OF ANALYSIS

Relaxation in glasses or quite general in disordered systems is typically probed by monitoring the evolution of a macroscopic quantity in response to the variation of an external control parameter, e.g., temperature. The study of enthalpy or volume release triggered by abruptly increasing the temperature or applying a heating rate to a system is the basis for understanding physical aging phenomena. The processes that govern physical aging are related to the

out-of-equilibrium dynamics of structural degrees of freedom enabling the system to approach a distinct constraint equilibrium state, metastable or true equilibrium, set by the variations of external control parameter(s). This scenario is the root cause of what is termed structural relaxation which typically involves nonequilibrium and nonlinear dynamics in disordered systems.^{4,20,48,49}

To interpret and understand structural relaxation, a variety of models have been devised to analyze data from relaxation and aging experiments. Most prominent are the Tool-Narayanaswamy-Moynihan (TNM),^{50–52} the Kovacs-Aklonis-Hutchinson-Ramos (KAHR),⁵³ and the Lunkenheimer-Wehn-Schneider-Loidl (LWSL)⁹ models. The latter is a phenomenological and simple tool, which is limited to analyze aging isotherms with emphasis on extracting very long relaxation time constants. The KAHR and TNM models assume that a single dynamical variable is sufficient to characterize the state of a system in a nonequilibrium situation. The standard TNM model is formulated in terms of a fictive temperature T_f to model the total deviation from equilibrium. Conceptually, this approach assumes that a homogeneous relaxation dynamics is operating where all relaxing units of the system follow the same nonexponential decay pattern and the characteristic relaxation time constant τ depends on real temperature and fictive temperature, i.e., $\tau = \tau(T, T_f)$. The latter accounts for the dependence of τ on structure or the configurational state.

The KAHR approach⁵³ is based on the premise of heterogeneous dynamics thereby supposing that the typically observed nonexponential relaxation patterns originate from an assemblage of individual domains, characterized by different relaxation time constants τ_i . The departure from equilibrium of each domain i is given by δ_i where $\sum_{i=1}^N \delta_i = \delta$ over all domains N represents the total departure from equilibrium in terms of enthalpy H : $\delta = H - H_\infty$, where H_∞ denotes the (constraint) equilibrium value the systems tends to in the long time limit. As a consequence, the distinct relaxation time constants τ_i depend on their individual δ_i values, i.e., $\tau_i = \tau_i(T, \delta_i)$. However, in a later step, the KAHR model assumes that the relaxation dynamics must depend on the overall state of a system but not on the specific values of each domain, resulting in $\tau_i = \tau_i(T, \delta)$. It follows that both models can be made mathematically equivalent, provided the Boltzmann superposition principle^{54,55} holds, which implies that in the linear response regime the response to a previously applied generalized force is not affected by a subsequent application and vice versa.¹¹ In fact, it is implied here that δ plays the same role as T_f in the TNM model and as a consequence, heterogeneous and homogeneous modeling of enthalpy relaxation becomes equivalent.

It follows from the formalism of the TNM and KAHR models that time temperature superposition (TTS) or thermorheological simplicity⁵⁴ and time aging-time superposition (TaTS)¹ should be valid. Both approaches are based on the assumption that upon relaxation the underlying shape of the relaxation time spectrum remains constant when external forces or fields, e.g., temperature and aging time t_e , vary. Considering relaxation time spectra, TTS requires that all relaxation times are identical functions of temperature. Technically, such a behavior enables to generate a master curve by shifting relaxation data, recorded over long time ($>10^5$ s) and for several different temperatures, along the time axis relative

to an unshifted reference temperature. Similarly, TaTS implies that an increase in aging time changes all relaxation times by exactly the same factor. It follows that the time evolution of relaxation data, taken at a given temperature and for a set of increasing aging times, can be mapped onto a master curve by horizontal shifts and stretches along the time axis.

In most cases, the models discussed above do not describe experimental data of glasses accurately and are not capable of discriminating between homogeneous or heterogeneous nature of the relaxation dynamics. This is essentially related to an observed response behavior, which deviates from linearity and violates time invariance of time constants. Since we are interested in modeling structural relaxation in NC materials, which are in contrast to glasses essentially heterogeneous—yet statistically homogeneous—materials, it seems evident that fictive temperature approaches must fail. In particular, the heterogeneous nature of the network of GBs can be imagined as an assemblage of a variety of structural units, reflecting the local fluctuations of overlapping potential fields of abutting and differently oriented crystallites. These structural units or domains are characterized by a site-specific deviation from local equilibrium, which entails that different domains own their individual δ_i -values.

To adapt to the nature of GBs, it is mandatory to employ a model that goes beyond the single dynamical variable approach. Therefore, we decided to follow the recommendations of the Kinetics Committee of the International Confederation for Thermal Analysis and Calorimetry (ICTAC)⁵⁶ to model and analyze the data obtained from thermal analysis methods. Since we are going to apply the kinetic approach to dilatometry data, where the evolution of linear strain is monitored as a function of different time-temperature protocols, we formulate the kinetic approach in terms of strain rate response; an adaption to calorimetry data is straightforward and could be introduced when required.

To handle the complexity of the relaxation process, we consider a distributed reactivity model that partitions the overall process into a set of independent and parallel reactions. As a start and for the sake of simplicity, we omit cross talking between different modes and neglect hierarchical reaction schemes where the activation of a specific mode(s) enables further modes.

The rate equation for overall strain evolution, $d\varepsilon/dt$, reads

$$\frac{d\varepsilon}{dt} = \sum_{i=1}^n k_i(T(t))f_i(\varepsilon_i(t)), \quad (1)$$

where $k_i(T(t))$ represents the temperature dependence of the process rate, and the function $f_i(\varepsilon_i(t))$ models the influence of strain conversion of the i th process on its conversion rate.

We implement $k_i(T(t))$ by an Arrhenius-type expression given as

$$k_i(T(t)) = \dot{\varepsilon}_{0,i}(T(t))\exp(-\Delta G_i^*/k_B T(t)). \quad (2)$$

The kinetic parameter ΔG_i^* denotes the Gibbs free energy of activation of the i th reaction. We distinguish free energies/enthalpies of activation (ΔG_i^* , ΔH_i^*) by an asterisk from free energy/enthalpy differences (ΔG , ΔH) related to different states of the system; $k_B T(t)$

has its usual meaning. The Gibbs free energy of activation is a lower bound for the Helmholtz free energy of activation $\Delta F_i^* = \Delta G_i^* + \Delta W$, where ΔW is the mechanical work provided by the stress/strain release from the nanocrystallites and GBs. This work term, or rather its decrease with proceeding relaxation, is a manifestation of the exhaustion of the driving forces for the relaxation. Moreover, the mere decrease of ΔW is sufficient to cause a distribution of ΔG_i^* parameters even if all ΔF_i^* were identical. The preexponential factor $\dot{\varepsilon}_{0,i}(T(t))$ differs from the usually taken constant reference strain rate for the following reasons. For thermally activated overcoming of energy barriers that manifest transformation dilatational strain $\Delta\varepsilon$, the deformation rate due to kinematically possible local dilatational relaxations is given as $\dot{\varepsilon}_{0,i}(T(t)) = c_i \Delta\varepsilon_i v_{c,i}(T(t))$.⁵⁷ Here, c_i represents the initial volume fraction of domains that take part in configurational transformation by operating in the i th reaction mode. The term $v_{c,i}(T(t))$ represents a cluster frequency—much smaller than the Debye frequency—involving many atoms that take part in a collective deformation event associated with the i th mode. The temperature dependence of $v_{c,i}(T(t))$ originates from the temperature dependence of the phonon dispersion relation.⁵⁸ Referring to the Bose statistics, it is straightforward to derive $v_{c,i}(T(t)) \propto 1/(\exp(\hbar\omega/k_B T(t)) - 1)$. Analyzing real data will in general not allow one to separate out the different factors that contribute to $\dot{\varepsilon}_{0,i}(T(t))$, instead we treat $\dot{\varepsilon}_{0,i}(T(t)) = \dot{\varepsilon}_{\max,i}/(\exp(\hbar\omega/k_B T(t)) - 1)$ as a temperature dependent parameter with $\dot{\varepsilon}_{\max,i}$ being the high temperature strain rate limit.

The second term in Eq. (1), the reaction model f_i , considers the contribution of the i th process to the overall strain rate depending on the already provided strain by this process in relation to its maximum possible strain contribution. We chose a decelerating reaction model according to the criteria in Ref. 56,

$$f_i(\varepsilon_i(t)) = 3 \left(1 - \frac{\varepsilon_i(t)}{\varepsilon_{\max,i}} \right)^{0.78}, \quad \varepsilon_i(t) \leq \varepsilon_{\max,i}, \quad (3)$$

where $\varepsilon_{\max,i}$ denotes the maximal possible strain contribution of the i th reaction mode. The exponent 0.78 was chosen in order to deliver the best fit to the data and takes care of the fact that processes decelerate more quickly for strains approaching $\varepsilon_{\max,i}$. In fact, the reaction model f_i can be interpreted as a model of the evolution of c_i , the volume fraction of domains that take part in the relaxation process i , resulting in $c_i(t) = c_i f_i(t)$.

In summary, each distinct reaction mode i is characterized by a triplet of kinetic parameters: ΔG_i^* , $\varepsilon_{\max,i}$, and $\dot{\varepsilon}_{\max,i}$. For any type of time-temperature protocol and given discrete triplets of kinetic parameters, differential equation (1) can be solved for $\varepsilon(t)$ numerically. Using the kinetic parameters as fit parameters, the so computed strains can be fitted simultaneously to several experiments carried out on the same material but with different time-temperature protocols. We like to emphasize that fitting only a single experiment generally produces unreliable results for the fit parameters.⁵⁶ Therefore, the kinetic parameters are not specific to a single experiment, but characterize the general relaxation behavior of the material—however, not necessarily the intrinsic relaxation mode of a physical domain. Hence, they rather represent effective

kinetic parameters that may deviate from the intrinsic heterogeneous relaxation dynamics.

IV. EXPERIMENTAL PROCEDURE

A. Sample synthesis

The NC Pd₉₀Au₁₀ samples were synthesized by inert gas condensation²¹ using an ultrahigh-vacuum system (base pressure 10⁻⁷ mbar) and thermal evaporation of high purity Pd and Au wires in a 6 mbar helium atmosphere. The nanocrystalline powder was subsequently transferred to a piston and anvil device and compacted under high vacuum (<10⁻⁶ mbar) at a pressure of 1.8 GPa for a time period of 30 s to obtain disk-shaped samples (pellets) with a diameter of 8 mm, a thickness of 500–600 μm, and an initial grain size of ≈10 nm.

It is a known fact that friction between the powder and the wall of the compaction tool leads to nonuniform applied stress and consequently to a nonuniform compaction of the NC pellet. To quantify the resulting circularly symmetric inhomogeneity in density, a sacrificial sample was gradually ground down to smaller diameters. After each step, the bulk density ρ_{bulk} of the remaining pellet, i.e., the density of the sample including closed porosity, was determined by the method of Archimedes⁵⁹ using a beam balance Sartorius S3D with a resolution of 1 μg and the reference media air and diethyl phthalate (DEP). From these data, the mean relative bulk density of every radial segment could be reconstructed, which is shown in Fig. 3.

B. Dilatometry

The macroscopic length change during thermal annealing was measured using a Netzsch TMA402 Hyperion dilatometer with a temperature range from -150 °C to 1000 °C. The specimens were positioned on a silica sample holder and contact was made by applying a force of 50 mN on a push rod with a circular contact area of 1 mm diameter. Thermal expansion of the silica sample

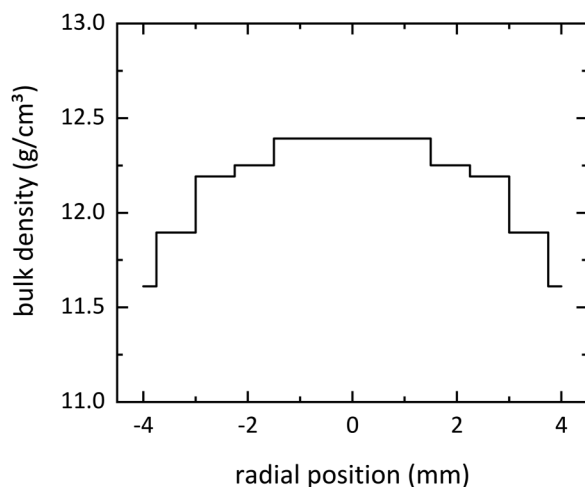


FIG. 3. Radial bulk density distribution of a nanocrystalline Pd₉₀Au₁₀ specimen with 8 mm diameter.

holder was corrected automatically via the built-in calibration function of the Netzsch Proteus Analysis software. To extract the irreversible share of the length change, the reversible thermal expansion was estimated by linear thermal expansion and subsequently subtracted from the measurement. The mean thermal expansion coefficient $\alpha = 12.5 \times 10^{-6} \text{ K}^{-1}$ was extracted from the reversible linear expansion of the specimen before and after relaxation. In the limited temperature range regarded in this study and compared to the magnitude of the relaxation effect, this approach is sufficiently accurate. The remaining irreversible length changes ΔL were related to initial length L_0 in measuring direction to obtain the corresponding engineering strain $\varepsilon = \Delta L/L_0$.

V. RESULTS AND DISCUSSION

To study the strain relaxation phenomenon, a NC Pd₉₀Au₁₀ pellet produced by IGC was cut into 4 quadratic pieces with 2 mm edge length and several rounded edge pieces (see Fig. 4). The 4 quadratic pieces from the center of the pellet are identified as samples A1–A4 and have a relatively uniform density due to their central position in the pellet (cf. Fig. 3). Beyond that, four extra samples B1–B4 from the edge of the pellet were also selected for analysis. Although chemically identical to set A, they have a significantly lower density and a more pronounced density gradient. In the framework set out in Fig. 2, the lower density of the B samples directly corresponds to higher (specific) volume, likewise to higher initially stored enthalpy or entropy, which effectively renders them into less structurally relaxed versions of the A samples.

Mounted in the dilatometer, samples A and B were subjected to 8 different time-temperature protocols [see Table I and Figs. 5(a) and 6(a)], respectively, and the resulting evolution of irreversible engineering strains due to structural relaxation is shown in Figs. 5(b) and 6(b) (solid lines). They invariably show a pronounced length reduction during annealing, where the respective strain evolution with time sensitively depends on the corresponding time-temperature protocol. The less dense B samples exhibit a

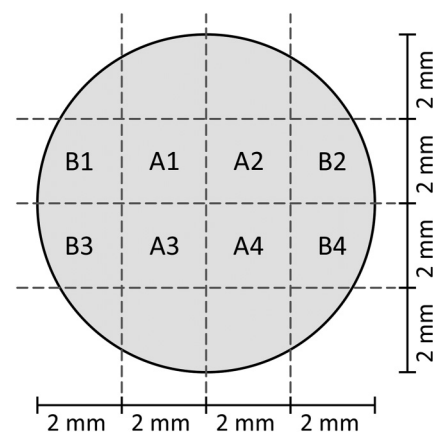


FIG. 4. Schematic representation of the partitioning of the as-received specimen into the different samples of the two sets A and B.

TABLE I. Time-temperature protocols of relaxation experiments. Heating segments are not strictly linear, the reported rates represent averages over the entire segments.

Sample	Segment	Duration (min)	Temperature (°C)	Rate (K/min)
A1	Heating	1072	21.4–124.7	0.096
	Isotherm	7737	124.7	...
A2	Heating	240	23.6–105.4	0.341
	Isotherm	8584	105.4	...
A3	Heating	55	26.9–86	1.075
	Isotherm	8772	86	...
A4	Heating	272	21.6–86	0.237
	Isotherm	4320	86	...
B1	Heating	20	23.1–120	4.845
	Isotherm	8800	120	...
B2	Heating	40	21.7–120	2.458
	Isotherm	1731	120	...
B3	Heating	29	21.8–95.7	2.548
	Isotherm	3168	95.7	...
B4	Heating	26	21.6–71.6	1.923
	Isotherm	1740	71.6	...
	Heating	4978	71.6–120	0.0097
	Isotherm	2077	120	...

higher total strain and less tendency to approach a steady state, so indicating that their initial (as-prepared) state resides farther away from equilibrium.

As introduced above (cf. Sec. III), strain data constitute the basis for analyzing thermal activation parameters. However, it is *a priori* unknown which number of terms i in Eq. (1) are required to adequately model the corresponding relaxation processes. Therefore, we performed a series of fits with increasing number of triplets to ascertain the convergence of the minimal sum of weighted quadratic deviations of the model from experiment (see Fig. 7). As it turns out, there is no significant improvement beyond the use of 8 triplets, so we restrict all further analysis to this number of triplets.

The experimentally observed strains for all time-temperature protocols could be modeled individually with very high accuracy. However, in order to achieve a similar level of agreement between model and experiment for a global fit of all samples from the sets A or B, respectively, we had to introduce an additional degree of freedom in the form of a compensation temperature $T_{c,x}$, where x is the number of the sample (here 1–4). This temperature modifies the experimentally observed temperature T according to $T'_x = T + T_{c,x}$, where T'_x is used instead of T for strain computation. The purpose of T_c is to compensate all relative variations in relaxation behavior between individual samples of a set. Such variations may originate from small deviations between corresponding δ_i -values. As only relative variations within a set are of relevance, we can freely choose the first sample in both sets as a reference sample so that $T_{c,1} = 0$ K and

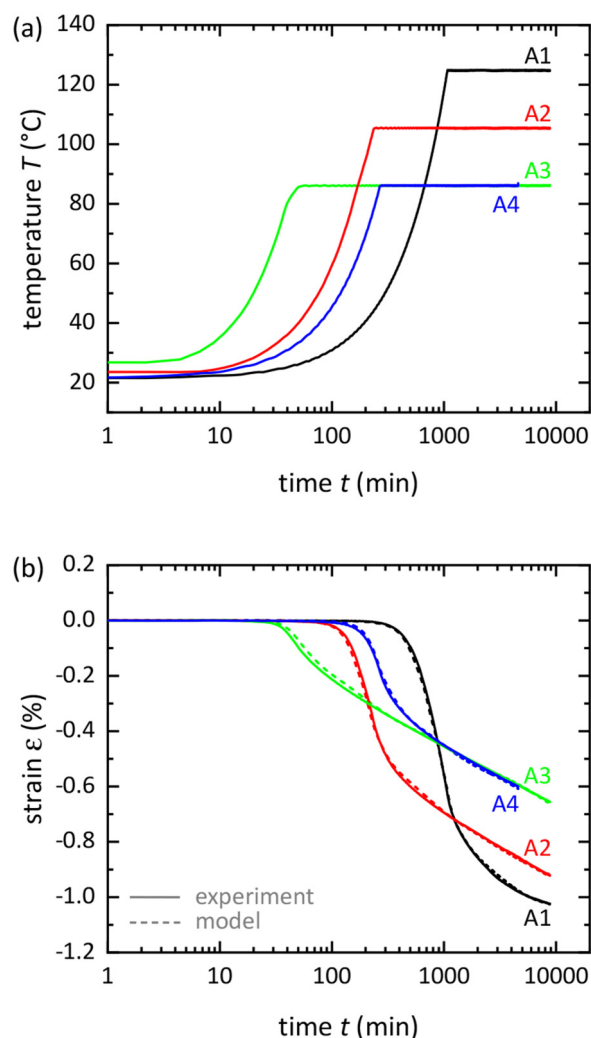


FIG. 5. (a) Evolution of temperature during dilatometry of all samples of set A. (b) Corresponding measured irreversible strain (solid lines) and modeled strain (dashed lines).

use the remaining 3 compensation temperatures as additional fit parameters the values of which are reported in Table II. More details of the fitting procedure are given in the Appendix.

The resulting global fits are shown as dashed lines in Figs. 5(b) and 6(b), and the corresponding activation parameter triplets are reported in Tables III and IV. To evaluate the impact of T_c on the modeled thermal activation, we straightforwardly calculate the corresponding relative change in the thermal energy term $\Delta Q/Q = (k_B T' - k_B T)/k_B T = T_c/T$, which quantifies the extend of statistical inhomogeneity in δ_i -values of different samples relative to the reference sample. We obtain upper bounds of $\Delta Q/Q$ for the center samples A of 1.8% and for the edge samples B of 4.1%, indicating an increased spread of inhomogeneity of initial states between samples of set B. Moreover, the larger radial density

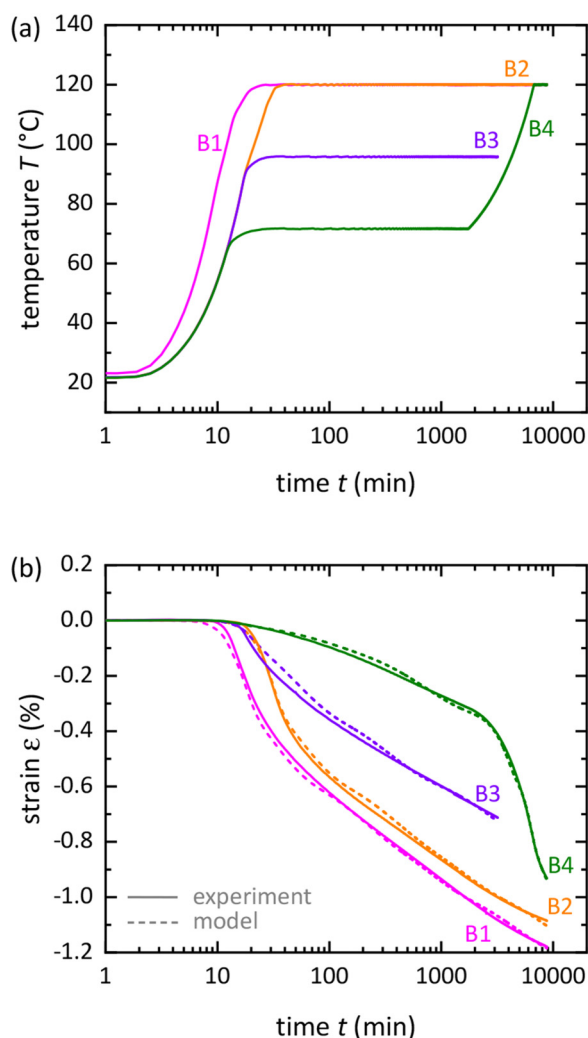


FIG. 6. (a) Evolution of temperature during dilatometry of all samples of set B. (b) Corresponding measured irreversible strain (solid lines) and modeled strain (dashed lines).

gradient across these samples (cf. Fig. 3) renders the dilatometer measurement sensitive to the exact positioning of the push rod, so additionally affecting the observed relaxation behavior and contributing to T_c .

The two sets of activation parameters (cf. Tables III and IV) unveil the following key feature. First, the spread in the Gibbs free energy of activation of sample set B expands over a larger range of values (0.84–1.25 eV) than that of set A (0.99–1.25 eV). We notice that their largest Gibbs free energies of activation are almost identical; however, B samples exhibit significantly smaller minimal values. Obviously, the larger amount of stored enthalpy (volume, entropy, etc.) in the initial state of B samples is correlated with a broadening of the activation energy spectrum toward the lower end. However, the total strain contribution $\varepsilon_{\max,i}$ of the two most

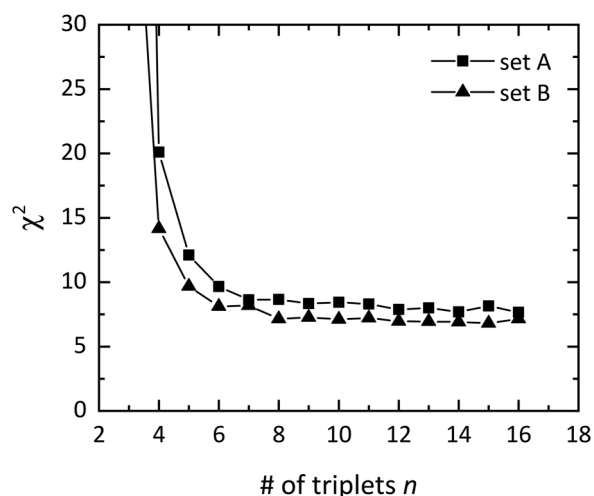


FIG. 7. Residual of the optimization function χ^2 as a function of the number of activation parameter triplets n (equivalent to the number of processes i) for sample sets A (squares) and B (triangles).

easily activated processes $i = 1$ and 2 is relatively small, thus limiting their impact to the early stages of relaxation. In fact, for the time-temperature protocols applied to the set of B samples, processes $i = 1$ and 2 only contribute to strain relaxation within the first 100 min; their effect is negligible beyond that time.

The second feature relates to the values of $\dot{\varepsilon}_{\max,i}$ and $\varepsilon_{\max,i}$ of the B samples, which are significantly larger than their counterparts in set A. We note that processes $i = 1$ and 2 operating in set B have no equivalent in set A and remain therefore unconsidered in what follows. Nevertheless, the second finding can only originate from the factors c_i and/or $\Delta\varepsilon_i$ entering the deformation rate $\dot{\varepsilon}_{0,i}(T(t))$ [cf. Eq. (2)]. Since c_i represents the volume fraction of domains that can undergo the relaxation process i and $\Delta\varepsilon_i$ the associated transformation dilatational strain, it becomes evident that the higher the volume fraction of in parallel relaxing domains is, the higher is the resulting strain rate as well as the maximally achievable total strain by this process. The same is true for an increase in the transformation dilatational strain. Consequently, the higher stored enthalpy (volume, entropy, etc.) of B samples correlates with a higher concentration of relaxation domains and/or

TABLE II. Compensation temperatures T_c for samples of sets A and B. See the text for further information.

Set A		Set B	
Sample	T_c (K)	Sample	T_c (K)
A1	0	B1	0
A2	5.19	B2	-7.24
A3	-1.16	B3	-5.01
A4	0.26	B4	-12.09

TABLE III. Kinetic parameters of sample set A. ΔG_i^* are Gibbs free energies of activation, $\epsilon_{\max,i}$ is the maximum strain contribution of process i to the overall strain, and $\dot{\epsilon}_{\max,i}$ is the high temperature strain rate limit.

Process i	ΔG_i^* (eV)	$\epsilon_{\max,i}$ (%)	$\dot{\epsilon}_{\max,i}$ ($10^8/s$)
1	0.991	-0.114	-1.875
2	1.014	-0.183	-1.964
3	1.069	-0.170	-1.893
4	1.153	-0.078	-1.929
5	1.153	-0.080	-1.982
6	1.179	-0.140	-2.000
7	1.234	-0.107	-1.911
8	1.246	-0.160	-1.946

higher transformation dilatational strain of these domains during relaxation. However, in the realm of the utilized model, it is impossible to discriminate between the two contributions.

A further, more technical aspect pertains to the existence of duplicate energy values (1.153 eV for A and 1.254 eV for B) in both sample sets. They coincide with comparatively low values for $\epsilon_{\max,i}$ whereas the maximum strain rates $\dot{\epsilon}_{\max,i}$ seem not affected. This is a clear indication that the choice of 8 triplets is already on the verge of overdetermination, where the effect of a single process is distributed among two separate processes. This reasoning becomes also evident from the small improvement in fit quality when increasing the number of triplets from 7 to 8 as displayed in Fig. 7.

As a matter of fact, we cannot guarantee completeness of this spectrum of activation free energies for the following fundamental reason: strain measurements span only a limited period of time. As a consequence, the relaxation process does not reach the regime of stagnation so causing a lack of information about the relaxation behavior for very long relaxation times. This regime is essentially characterized by the highest activation energies which, therefore, may elude our analysis. Resolving this problem requires increasing the measuring time to the completion of the relaxation process, provided that this state does exist.

Regarding the pertinent literature dealing with metallic systems, we are to the best of our knowledge only aware of the work of Atzmon and co-workers.^{60,61} They analyzed the time

TABLE IV. Kinetic parameters of sample set B. ΔG_i^* are Gibbs free energies of activation, $\epsilon_{\max,i}$ is the maximum strain contribution of process i to the overall strain, and $\dot{\epsilon}_{\max,i}$ is the high temperature strain rate limit.

Process i	ΔG_i^* (eV)	$\epsilon_{\max,i}$ (%)	$\dot{\epsilon}_{\max,i}$ ($10^8/s$)
1	0.839	-0.014	-0.129
2	0.881	-0.047	-1.132
3	0.899	-0.216	-0.125
4	1.057	-0.237	-2.850
5	1.131	-0.182	-2.782
6	1.171	-0.219	-2.646
7	1.254	-0.151	-2.714
8	1.254	-0.144	-2.579

dependent component of the room temperature deformation of Al-based metallic glass at strains far below yield. Their results are compatible with the idea that the buildup of back stresses in the elastic matrix leads to fully reversible anelastic behavior that originates from localized and isolated shear transformations, the characteristic flow event in metallic glasses. Direct spectrum analysis of the strain vs time data yielded relaxation-time spectra, which consisted of a hierarchy of peaks each characterized by an effective and also distinct time constant. Each peak value was modeled by a linear-dashpot-and-spring model to yield several properties of shear transformations. Interestingly, the number of distinct peaks amounted to 7–8 and so compares favorably with the number of triplets we found in our analysis; however, further studies are needed to elucidate whether this finding has a common background or is just a coincidence. In line with this reasoning, Atzmon *et al.* identified 7 distinct Helmholtz free energies of activation ΔF^* , which were related to different shear transformation events and varied between 0.85 eV and 1.26 eV per atom. However, these values are not directly comparable with the Gibbs free energies of activation ΔG^* we determined for NC PdAu. Even if the mechanical work term that needs to be added to ΔG^* to allow for comparison with ΔF^* were negligibly small, Young's modulus of PdAu alloys is more than two times larger than the value of the Al-based metallic glass and therefore prohibits meaningful comparison.

VI. SUMMARY AND CONCLUSIONS

Materials residing in nonequilibrium states tend to spontaneously evolve toward a temporally distant equilibrium state, whenever it is kinetically facilitated at a given temperature. The concomitant slow change of material properties was termed (physical) aging or (structural) relaxation—just using the most prominent nomenclature. Aging is essentially related to changes in the relaxation times of microscopic processes underlying the system's structural relaxation dynamics toward lower-energy states. Studying aging phenomena was and still is an active field of the glass community, covered by a number of excellent review articles.^{1,2,4,15–19} We like to emphasize that aging is not restricted to the glassy state but is a manifestation of all kinds of disordered materials. In this study, we deal with NC materials that are heterogeneous materials where disorder (atomic-site mismatch) predominantly prevails in the core region of the three-dimensional network of grain boundaries and triple junctions. We concentrate on the low end of the nanoscale ($D \approx 10$ nm) where the interfacial phase becomes a prominent element of microstructure.

Upon aging, NC materials respond to applied stimuli with a behavior deviating from linearity and violating time invariance of the relaxation time constants. Therefore, the commonly used approaches, the LWSL,⁹ TNM,^{50–52} or KAHR⁵³ models, likewise, the empirical fitting of relaxation data with stretched exponentials,^{62,63} are not adequate to model structural relaxation in NC materials, which require to take into account that deviation from global equilibrium entails a spectrum/distribution of site-specific deviations from local equilibrium.

In this study, we managed for the first time to analyze the structural relaxation kinetics in NC PdAu alloys with a grain size of ≈ 10 nm based on a distributed reactivity model.⁵⁶ It partitions the

overall process into a set of independent and parallel reactions for arbitrary time-temperature protocols. Each individual reaction mode is represented by a triplet of effective kinetic parameters the whole set of which characterizes the overall relaxation behavior of the material. Different from the commonly assumed phenomenological stretched-exponential behavior,^{62,63} the spectrum of kinetic parameters was obtained without making any *a priori* assumptions with regard to their distribution functions, etc. Moreover, these parameters have a well defined physical meaning given by the utilized reactivity model.

The applied approach of modeling relaxation dynamics, although yielding effective kinetic parameters, is sensitive to the intrinsic heterogeneous relaxation dynamics. In fact, we could show that the set of kinetic parameters is significantly influenced—apart from material selection—by preparation history and sample processing of nominally the same material. As expected, the investigated NC PdAu alloy violates time temperature superposition and time aging-time superposition, revealing the actual complexity of the relaxation behavior already on a macroscopic level. It would be desirable to also apply this way of modeling aging behavior to metallic glasses to overcome the pitfalls related to analyze the time evolution of isotherms individually.

Greater insights will be obtained by analyzing configurational enthalpy, volume, and elastic moduli changes between different states assumed by the system along its path to stable equilibrium. In fact, we are interested in to quantitatively extract the potential energy bias toward the global minimum. In a forthcoming paper, we will address this issue and then combine kinetic and state analysis. This will enable to reconstruct the effective energy landscape of the system and so advance the understanding of relaxation in nanocrystalline materials.

ACKNOWLEDGMENTS

The authors acknowledge the financial support of the Deutsche Forschungsgemeinschaft (No. BI 385/18-2). They thank Michael Atzmon (University of Michigan) for fruitful discussions.

APPENDIX: FITTING PROCESS

In order to achieve a rapid and reliable convergence in the fitting process, all three thermal activation parameters have to be constrained to physically reasonable ranges. It is furthermore obligatory to choose reasonable start values for all parameters. In the following, we will report these values along with the underlying physical reasoning.

Start values for the maximal achievable strain per process $\varepsilon_{\max,i}$ were straightforwardly chosen by dividing the largest experimentally observed strain by the number of modeled processes i . The fitting procedure then could refine $\varepsilon_{\max,i}$ in the interval $(-5\%, 0)$.

To estimate values for the maximum strain rate $\dot{\varepsilon}_{\max,i}$, we refer to the relation $\dot{\varepsilon}_{0,i}(T(t)) = c_i \Delta E_i v_{c,i}(T(t))$,⁵⁷ which can be split in the two factors $c_i \Delta E_i$ and $v_{c,i}(T(t))$. With the previous reasoning, we estimate $\varepsilon_{\max,i} = c_i \Delta E_i \approx -1\%$. To assess the value of $v_{c,i}$, we assume that the phonon spectrum of the GB phase is identical to that of the crystalline phase, which results in an overestimation of $v_{c,i}$ by less than an order of magnitude. We further postulate that

the spatial extent of the coherent movement of atoms for thermal activation spans at least the width of the GB (≈ 1 nm). This imposes a limit on the phonon spectrum of Pd⁶⁴ that goes along with reduced wave vectors ξ smaller than 0.2; we note that Pd exhibits higher phonon frequencies than gold. Overall, this leads to the upper bound estimate $v_{c,i} \leq 10^{12} \text{ s}^{-1}$ resulting in $\dot{\varepsilon}_{0,i} \leq 10^9 \text{ s}^{-1}$. Consequently, 10^9 s^{-1} was chosen as a start value for $\dot{\varepsilon}_{\max,i}$, which could be refined in the interval $(10^7 \text{ s}^{-1}, 2 \times 10^9 \text{ s}^{-1})$.

The start value of ΔG_i^* was located in the range of 0.9–1.1 eV that could be varied during fitting from 0.75 eV to 1.375 eV.

Lastly, the bounds for T_c were assumed to lie in the interval $(-20 \text{ K}, 20 \text{ K})$ and the start value for T_c was set to 0 K.

REFERENCES

- 1L. C. E. Struik, *Physical Aging in Amorphous Polymers and Other Materials* (Elsevier Scientific Publishing Company, 1978).
- 2I. M. Hodge, "Enthalpy relaxation and recovery in amorphous materials," *J. Non Cryst. Solids* **169**, 211 (1994).
- 3W. Klement, R. H. Willens, and P. Duwez, "Non-crystalline structure in solidified gold-silicon alloys," *Nature* **187**, 869 (1960).
- 4C. A. Angell, K. L. Ngai, G. B. McKenna, P. F. McMillan, and S. W. Martin, "Relaxation in glassforming liquids and amorphous solids," *J. Appl. Phys.* **88**, 3113 (2000).
- 5A. L. Greer, "Metallic glasses," in *Physical Metallurgy*, 5th ed., edited by D. E. Laughlin and K. Hono (Elsevier, Oxford, 2014), Chap. 4, p. 305.
- 6D. Deng and A. S. Argon, "Structural relaxation and embrittlement of Cu₅₉Zr₄₁ and Fe₈₀B₂₀ glasses," *Acta Metall.* **34**, 2011 (1986).
- 7X. Shi, A. Mandanici, and G. B. McKenna, "Shear stress relaxation and physical aging study on simple glass-forming materials," *J. Chem. Phys.* **123**, 174507 (2005).
- 8R. L. Leheny and S. R. Nagel, "Frequency-domain study of physical aging in a simple liquid," *Phys. Rev. B* **57**, 5154 (1998).
- 9P. Lunkenheimer, R. Wehn, U. Schneider, and A. Loidl, "Glassy aging dynamics," *Phys. Rev. Lett.* **95**, 055702 (2005).
- 10G. W. Scherer, "Theories of relaxation," *J. Non Cryst. Solids* **123**, 75 (1990).
- 11S. K. S. Mazinani and R. Richert, "Enthalpy recovery in glassy materials: Heterogeneous versus homogenous models," *J. Chem. Phys.* **136**, 174515 (2012).
- 12G. B. McKenna, "Mechanical rejuvenation in polymer glasses: Fact or fallacy?," *J. Phys. Condens. Matter* **15**, S737 (2003).
- 13P. de Hey, J. Sietsma, and A. van den Beukel, "Structural disordering in amorphous Pd₄₀Ni₄₀P₂₀ induced by high temperature deformation," *Acta Mater.* **46**, 5873 (1998).
- 14Y. Sun, A. Concustell, and A. L. Greer, "Thermomechanical processing of metallic glasses: Extending the range of the glassy state," *Nat. Rev. Mater.* **1**, 16039 (2016).
- 15V. Lubchenko and P. G. Wolynes, "Theory of aging in structural glasses," *J. Chem. Phys.* **121**, 2852 (2004).
- 16M. D. Ediger, "Spatially heterogeneous dynamics in supercooled liquids," *Annu. Rev. Phys. Chem.* **51**, 99 (2000).
- 17B. Ruta, E. Pineda, and Z. Evenson, "Relaxation processes and physical aging in metallic glasses," *J. Phys. Condens. Matter* **29**, 503002 (2017).
- 18M. Micoulaut, "Relaxation and physical aging in network glasses: A review," *Rep. Prog. Phys.* **79**, 066504 (2016).
- 19I. Gallino and R. Busch, "Relaxation pathways in metallic glasses," *JOM* **69**, 2171 (2017).
- 20E. Donth, *The Glass Transition: Relaxation Dynamics in Liquids and Disordered Materials*, Springer Series in Materials Science Vol. 48 (Springer, Berlin, 2001).
- 21R. Birringer, "Nanocrystalline materials," *Mater. Sci. Eng. A* **117**, 33 (1989).

- ²²C. E. Krill and R. Birringer, "Estimating grain-size distributions in nanocrystalline materials from x-ray diffraction profile analysis," *Philos. Mag. A* **77**, 621 (1998).
- ²³A. Tschöpe and R. Birringer, "Thermodynamics of nanocrystalline platinum," *Acta Metall. Mater.* **41**, 2791 (1993).
- ²⁴A. P. Sutton and R. W. Balluffi, *Interfaces in Crystalline Materials*, Oxford Classic Texts in the Physical Sciences (Oxford University Press, Oxford, 2006).
- ²⁵M. Ames, J. Markmann, R. Karos, A. Michels, A. Tschöpe, and R. Birringer, "Unraveling the nature of room temperature grain growth in nanocrystalline materials," *Acta Mater.* **56**, 4255 (2008).
- ²⁶R. Birringer, M. Hoffmann, and P. Zimmer, "Interface stress in polycrystalline materials: The case of nanocrystalline Pd," *Phys. Rev. Lett.* **88**, 206104 (2002).
- ²⁷C. E. Krill and R. Birringer, "Investigations of grain-boundary structure and stability in nanocrystalline Pd," *Mater. Sci. Forum* **225–227**, 263 (1996).
- ²⁸D. Jang and M. Atzmon, "Grain-boundary relaxation and its effect on plasticity in nanocrystalline Fe," *J. Appl. Phys.* **99**, 083504 (2006).
- ²⁹J. Löffler and J. Weissmüller, "Grain-boundary atomic structure in nanocrystalline palladium from x-ray atomic distribution functions," *Phys. Rev. B* **52**, 7076 (1995).
- ³⁰A. Tschöpe, R. Birringer, and H. Gleiter, "Calorimetric measurements of the thermal relaxation in nanocrystalline platinum," *J. Appl. Phys.* **71**, 5391 (1992).
- ³¹R. Birringer, C. E. Krill, and M. Klingel, "Orientation-phase-space-averaged properties of grain boundaries," *Philos. Mag. Lett.* **72**, 71 (1995).
- ³²A. Hasnaoui, H. Van Swygenhoven, and P. Derlet, "Cooperative processes during plastic deformation in nanocrystalline fcc metals: A molecular dynamics simulation," *Phys. Rev. B* **66**, 184112 (2002).
- ³³K. L. Merkle, "Quantification of atomic-scale grain boundary parameters by high-resolution electron microscopy," *Ultramicroscopy* **40**, 281 (1992).
- ³⁴A. J. Detor and C. A. Schuh, "Microstructural evolution during the heat treatment of nanocrystalline alloys," *J. Mater. Res.* **22**, 3233 (2007).
- ³⁵B. Oberdorfer, D. Setman, E.-M. Steyskal, A. Hohenwarther, W. Sprengel, M. Zehetbauer, R. Pippin, and R. Würschum, "Grain boundary excess volume and defect annealing of copper after high-pressure torsion," *Acta Mater.* **68**, 189 (2014).
- ³⁶T. J. Rupert, J. R. Trelewicz, and C. A. Schuh, "Grain boundary relaxation strengthening of nanocrystalline Ni-W alloys," *J. Mater. Res.* **27**, 1285 (2012).
- ³⁷D. P. B. Aji and G. P. Johari, "Kinetic-freezing and unfreezing of local-region fluctuations in a glass structure observed by heat capacity hysteresis," *J. Chem. Phys.* **142**, 214501 (2015).
- ³⁸M. Grewer, J. Markmann, R. Karos, W. Arnold, and R. Birringer, "Shear softening of grain boundaries in nanocrystalline Pd," *Acta Mater.* **59**, 1523 (2011).
- ³⁹A. Leibner, C. Braun, J. Heppe, M. Grewer, and R. Birringer, "Plastic yielding in nanocrystalline Pd-Au alloys mimics universal behavior of metallic glasses," *Phys. Rev. B* **91**, 174110 (2015).
- ⁴⁰A. Stukowski, J. Markmann, J. Weissmüller, and K. Albe, "Atomistic origin of microstrain broadening in diffraction data of nanocrystalline solids," *Acta Mater.* **57**, 1648 (2009).
- ⁴¹A. Leonardi, M. Leoni, and P. Scardi, "Atomistic interpretation of microstrain in diffraction line profile analysis," *Thin Solid Films* **530**, 40 (2013).
- ⁴²A. Michels, C. E. Krill, H. Ehrhardt, R. Birringer, and D. T. Wu, "Modelling the influence of grain-size-dependent solute drag on the kinetics of grain growth in nanocrystalline materials," *Acta Mater.* **47**, 2143 (1999).
- ⁴³C. Braun, J. M. Dake, C. E. Krill, and R. Birringer, "Abnormal grain growth mediated by fractal boundary migration at the nanoscale," *Sci. Rep.* **8**, 1592 (2018).
- ⁴⁴C. E. Krill III, H. Ehrhardt, and R. Birringer, "Thermodynamic stabilization of nanocrystallinity," *Z. Metallkd.* **96**, 1134 (2005).
- ⁴⁵H. Gleiter, "Nanostructured materials: Basic concepts and microstructure," *Acta Mater.* **48**, 1 (2000).
- ⁴⁶R. Z. Valiev, R. K. Islamgaliev, and I. V. Alexandrov, "Bulk nanostructured materials from severe plastic deformation," *Prog. Mater. Sci.* **45**, 103 (2000).
- ⁴⁷R. Birringer, M. Hoffmann, and P. Zimmer, "Interface stress in nanocrystalline materials," *Z. Metallkd.* **94**, 1052 (2003).
- ⁴⁸R. Richert, "Perspective: Nonlinear approaches to structure and dynamics of soft materials," *J. Chem. Phys.* **149**, 240901 (2018).
- ⁴⁹R. Richert, "Physical aging and heterogeneous dynamics," *Phys. Rev. Lett.* **104**, 085702 (2010).
- ⁵⁰A. Q. Tool, "Relation between inelastic deformability and thermal expansion of glass in its annealing range," *J. Am. Ceram. Soc.* **29**, 240 (1946).
- ⁵¹O. S. Narayanaswamy, "A model of structural relaxation in glass," *J. Am. Ceram. Soc.* **54**, 491 (1971).
- ⁵²C. T. Moynihan, P. B. Macedo, C. J. Montrose, C. J. Montrose, P. K. Gupta, M. A. DeBolt, J. F. Dill, B. E. Dom, P. W. Drake, A. J. Easteal, P. B. Elterman, R. P. Moeller, H. Sasabe, and J. A. Wilder, "Structural relaxation in vitreous materials," *Ann. N. Y. Acad. Sci.* **279**, 15 (1976).
- ⁵³A. J. Kovacs, J. J. Aklonis, J. M. Hutchinson, and A. R. Ramos, "Isobaric volume and enthalpy recovery of glasses. II. A transparent multiparameter theory," *J. Polym. Sci. B Polym. Phys.* **34**, 2467 (1996).
- ⁵⁴J. D. Ferry, *Viscoelastic Properties of Polymers*, 3rd ed. (Wiley, 1980).
- ⁵⁵A. Shukla and Y. M. Joshi, "Boltzmann superposition principle for a time-dependent soft material: Assessment under creep flow field," *Rheol. Acta* **56**, 927 (2017).
- ⁵⁶S. Vyazovkin, A. K. Burnham, J. M. Criado, L. A. Pérez-Maqueda, C. Popescu, and N. Sbirrazzuoli, "ICTAC Kinetics Committee recommendations for performing kinetic computations on thermal analysis data," *Thermochim. Acta* **520**, 1 (2011).
- ⁵⁷A. S. Argon, *Strengthening Mechanisms in Crystal Plasticity*, 1st ed., Oxford Series on Materials Modelling Vol. 4 (Oxford University Press, Oxford, 2008).
- ⁵⁸N. W. Ashcroft and N. D. Mermin, *Solid State Physics* (Cengage Learning, 1976).
- ⁵⁹M. Hoffmann and R. Birringer, "Elastic and plastic behavior of submicrometer-sized polycrystalline NiAl," *Acta Mater.* **44**, 2729 (1996).
- ⁶⁰J. D. Ju, D. Jang, A. Nwankpa, and M. Atzmon, "An atomically quantized hierarchy of shear transformation zones in a metallic glass," *J. Appl. Phys.* **109**, 053522 (2011).
- ⁶¹M. Atzmon and J. D. Ju, "Microscopic description of flow defects and relaxation in metallic glasses," *Phys. Rev. E* **90**, 042313 (2014).
- ⁶²R. Kohlrausch, "Theorie des elektrischen Rückstandes in der Leidener Flasche," *Ann. Phys. Chem.* **91**, 56 (1854).
- ⁶³M. Atzmon, "The pitfalls of empirical fitting of glass relaxation data with stretched exponents," *J. Appl. Phys.* **123**, 065103 (2018).
- ⁶⁴A. P. Müller and B. N. Brockhouse, "Anomalous behavior of the lattice vibrations and the electronic specific heat of palladium," *Phys. Rev. Lett.* **20**, 798 (1968).